The Effect of Alzheimer's Aβ Aggregation State on the Permeation of Biomimetic Lipid Vesicles

Thomas L. Williams,[†] Iain J. Day,[‡] and Louise C. Serpell*,[†]

[†]*John Maynard Smith Building, School of Life Sciences, University of Sussex, Falmer, East Sussex, BN1 9QG, United Kingdom, and* [‡]*Department of Chemistry, School of Life Sciences, University of Sussex, Falmer, East Sussex, BN1 9QG, United Kingdom*

Alzheimer's disease is characterized by the aggregation and deposition of the Aβ peptide. This 40 or 42 residue peptide is the product of the proteolysis of the amyloid precursor protein membrane protein and is able to assemble to form ordered, stable amyloid fibrils as well as small, soluble, and potentially cytotoxic oligomers. The toxicity of the oligomers may be associated with the ability to bind to and affect the integrity of lipid membranes. In this novel work, we have monitored and compared the ability of the potent Aβ42 peptide, the less amyloidogenic Aβ40 peptide, and a variant with reduced amyloidogenicity to bind to and affect the integrity of membranes using dye-filled synthetic vesicles. We reveal that the potency of the assemblies reduces with incubation time of the peptide and that maximal effect occurs when a particular species is apparent by electron microscopy. We have investigated the effect of lipid vesicle composition, and our results suggest that charge on the vesicles is important and that binding may partly be mediated by the GM1 ganglioside receptors expressed in the outer leaflet of vertebrate membranes.

Introduction

Alzheimer's disease (AD) is characterized by a significant loss of neurons and by the deposition of extracellular amyloid fibrils in neuritic plaques and intraneuronal neurofibrillary tangles.[1] Neuritic plaques appear as star-shaped structures consisting of a central core of extracellular, fibrillar amyloid encompassing dystrophic nerve endings (neurites) and are composed of the amyloidogenic peptide, Aβ.[2] The formation of neuritic plaques is believed to be gradual, and to contain a greater abundance of Aβ42 compared to the shorter Aβ40. Aβ is able to form a number of assembly intermediates from low molecular weight oligomers, protofibrils, to mature amyloid fibrils.[3,4] The Aβ40 and Aβ42 variants are the predominant forms of Aβ in normal non-demented brains, comprising 50 and 23% of total soluble Aβ, respectively. These ratios of soluble Aβ40 and Aβ42 decrease to 2.7 and 0.7% in AD brains, respectively.[5] In vitro studies show that Aβ42 aggregates more rapidly compared to Aβ40. The faster aggregation propensity of Aβ42 is believed to be due to the additional hydrophobic isoleucine and alanine residues at positions 41 and 42, and is not a consequence of peptide length as substitution of these two residues with hydrophilic amino acids resulted in a decrease in aggregation kinetics.[6] The transient nature of Aβ assemblies remains a pivotal challenge in determining the toxicity of the peptide toward cells, and it is still controversial as to whether oligomeric or fibrillar amyloid is the toxic species, as well as the resulting mechanisms of toxicity.

Certain key regions within the amino acid sequence of Aβ have a profound effect on the aggregation propensity of the peptide. Mutation of the phenylalanine20 residue to the hydrophilic glutamic acid residue in the Aβ sequence has been reported to reduce the aggregation propensity of the peptide. In vivo studies with flies expressing Glu20 Aβ42 showed no signs of amyloid deposition at 20 days, and no visible deposits were detected in vivo despite the Glu20 Aβ42 peptide being capable of forming fibrils in vitro. This was attributed to the Glu20 mutation reducing the aggregation propensity of Aβ42 sufficiently enough to allow the flies to clear the peptide and thus to prevent accumulation of the slowly fibrillizing peptide.[7]

The binding and effect of Aβ on cellular membranes has been implicated in Aβ toxicity. Aβ has been shown to have an affinity for cellular membranes, which is unsurprising in light of its premodification processing from the integral membrane protein, amyloid precursor protein (APP).[8] The peptide contains two major hydrophobic sequences that account for 38% of the hydrophobicity profile centered around the LVFFA motif at residues 17−21 and Met35 at the C-terminus. Both of these hydrophobic motifs have been shown to be important in modulating fibrillization and hydrophobic interactions. The C-terminal residues are thought to form a hydrophobic core that stabilizes the peptide[9] and also causes the burial of Aβ within synthetic vesicle bilayers.[10] Moreover, the penetration of metal-bound Aβ can propagate oxidative damage from the methionine to the membrane, potentially causing oxidative damage and neurotoxicity.[11] The central hydrophobic core of Aβ40 and

(1) Glenner, G. G.; Wong, C. W. *Biochem. Biophys. Res. Commun.* **1984**, *120*, 885–890.
(2) Ng, H. K.; Chan, W. Y. *J. Hong Kong Med. Assoc.* **1993**, *45*, 33–39.
(3) Ward, R. V.; Jennings, K. H.; Jepras, R.; Neville, W.; Owen, D. E.; Hawkins, J.; Christie, G.; Davis, J. B.; Karran, E. H.; Howlett, D. R. *Biochem. J.* **2000**, *348*, 137–144.
(4) Bitan, G.; Kirkitadze, M. D.; Lomakin, A.; Vollers, S. S.; Benedek, G. B.; Teplow, D. B. *Proc. Natl. Acad. Sci. U.S.A.* **2003**, *100*, 330–335.
(5) Wang, J.; Dickson, D. W.; Trojanowski, J. Q.; Lee, V. M-Y. *Exp. Neurol.* **1999**, *158*, 328–337.
(6) Kim, W.; Hecht, M. H. *J. Biol. Chem.* **2005**, *280*, 35069–25076.

(7) Luheshi, L. M.; Tartaglia, G. G.; Brorsson, A.-C.; Pawar, A. P.; Watson, I. E.; Chiti, F.; Vendruscolo, M.; Lomas, D. A.; Dobson, C. M.; Crowther, D. C. *PLoS Biol.* **2007**, *5*, 2493–2500.
(8) Selkoe, D. J. *J. Physiol. Rev.* **2001**, *81*, 741–766.
(9) Shen, L.; Ji, H.-F.; Zhang, H.-Y. *J. Phys. Chem. B.* **2008**, *112*, 3164–3167.
(10) Curtain, C. C.; Ali, F.; Volitakis, I.; Chernyl, R. A.; Norton, R. S.; Beyreuther, K.; Barrow, C. J.; Masters, C. L.; Bush, A. L.; Barnham, K. J. *J. Biol. Chem.* **2001**, *276*, 20466–20478.
(11) Kanski, J.; Aksenova, M.; Butterfield, D. A. *Neurotox. Res.* **2002**, *4*, 219–223.

Aβ42 between residues 17−21 demonstrates a high propensity to interact with other regions of the peptide, in particular with the C-terminus, and may promote intermolecular contacts by driving the exclusion of water molecules between monomers.[12]

Biological membranes are complex mixtures of phosphorylated and glycolysated proteins and lipids, which are also pivotal for the correct functioning of the biological membranes. Gangliosides are found throughout vertebrates and expressed in the outer leaflet of plasma membranes. They are glycosphingolipids that contain a hydrophobic ceramide and hydrophilic sialic acid moieties, whereby the ceramide portion of the ganglioside is embedded within the membrane leaflet, while the negatively charged oligosaccharide chain is exposed to the external environment.[13] Moreover, they have been reported to serve a variety of functions, including as cell type-specific markers, differentiation and developmental markers, receptors, and as mediators of cell adhesion.[14] Ganglioside expression is stringently regulated, and their quantities vary between different cell types and within cells during cell maturation and differentiation. GM1 is mainly found within plasma membranes and is know to cluster and form lipid rafts within membranes. GM1 proportions within membranes vary and have been reported to represent between 0.5 and 13% w/w of the membrane.[15−17] The ability of GM1 to associate with Aβ has been reported, and it has been shown that Aβ40 bound to GM1 with a dissociation constant of $K_D = 1.4 \times 10^{-6}$ mol·dm^{-3}.[18] In the same study, they also showed that Aβ40 demonstrates a significantly lower binding affinity for the hydrophilic sialic acid moiety ($K_D = 218 \times 10^{-6}$ mol·dm^{-3}) compared to the hydrophobic ceramide moiety ($K_D = 7 \times 10^{-6}$ mol·dm^{-3}), suggesting that the association between GM1 and Aβ is a consequence of hydrophobic and electrostatic interactions.

Lipid vesicles have previously been used to study the membrane binding abilities of amyloid, typically focusing on fibrillar states and the determination of binding constants. Studies of different amyloid forming peptides using circular dichroism have shown that negatively charged lipids induce a random-coil to β transition in the Aβ25−35 fragments.[19] Further data has also shown that electrostatically driven conformational changes from random-coil through α-helical intermediates to β-sheet fibrils have been followed upon the binding of the amyloidogenic peptide MEDIN to negatively charged and neutral lipid vesicles.[20] Membranes have been shown to play a significant role in the aggregation of the diabetes type II related islet amyloid polypeptide (IAPP), and lipid-only catalyzed aggregation resulted in a 10-fold increase in the rate of IAPP fibrillization at substoichiometric amounts of lipid.[21] Membrane associated IAPP fibrillization was shown to be catalytic, as the membrane was neither consumed nor destroyed in spite of IAPP causing membrane distortion and disruption. The catalytic activities of the lipid membrane toward IAPP fibrillization have been attributed to the increasing local concentration of the IAPP and alignment of the protein molecules at the membrane surface[22] as well as attributed to stabilizing a critical α-helical intermediate species.[23]

Many of the studies performed on examining Aβ interactions with lipids were done prior to advances in understanding the importance of removing preaggregated species from synthetic peptides. Recently, it has become clear that Aβ is able to assemble to form many different assembled structures on (or off) the pathway to amyloid fibril formation. It is still unclear which of these species interact with membranes and whether this may cause disruption of the bilayer, leading to a disruption of membrane integrity. Here we have utilized large unilamellar vesicles (LUV) encapsulating a self-quenching fluorescent dye (calcein) as a simple biomimetic model alternative to in vivo natural cell membranes, effectively allowing us to monitor amyloid-induced membrane permeation. As calcein leaks from the internal aqueous space of the lipid vesicles it becomes diluted and dequenched, thereby causing an increase in fluorescence. The calcein release assay has previously been employed to monitor the liposomal leakage induced by the C-terminal fragment of Aβ, where it was demonstrated that Aβ29−42 caused around 30% more calcein release compared to Aβ12−42.[24] However, these fragments are not physiologically relevant to Alzheimer's disease. The Subramaniam group have used the calcein leakage assay to show a concentration dependent α-synuclein induced disruption of phosphatidylglycerol vesicles, and that the aggregation state of the peptide can affect the extent of dye release.[25]

Here, for the first time, we examine the in vitro interaction between two *physiologically relevant* Aβ peptide variants and biomimetic membrane models, as membranes are key to the integrity of all cells and if compromised will certainly cause debilitating effects. Here we explore the effect of aggregation state on the ability of wild-type Aβ42, the predominant Aβ variant found in Alzheimer's disease, to disrupt synthetic vesicles and reveal that as the peptide assembles, its ability to permeate the membranes decreases. This ability is compared to wild-type Aβ40, and a slower fibrillizing variant, Aβ40 Glu20. Early oligomers showed a significant capacity to cause leakage of the encapsulated calcein compared to fibrillar and slowly fibrillizing peptides. The removal of the GM1 ganglioside from the vesicle bilayer caused significant reduction in Aβ permeation of the membrane compared to bilayers with GM1.

Experimental Section

Amyloid Peptides. Lyophilized Aβ(1−40) (referred to as Aβ40) trifluoroacetate salt, > 95% purity, was purchased from Biosource (Camarillo, CA, USA). Lyophilized Aβ(1−40) Glu^{20} (referred to as Aβ40 Glu20), > 90% purity, was purchased from Bachem AG (Bubendorf, Switzerland). Aβ(1−42) HFIP (referred to as Aβ42), > 97% purity, was purchased from rPeptide (Bogart, GA, USA). All peptides were used without further purification.

Peptide Preparation. All three peptides—Aβ42, Aβ40, and Aβ40 Glu20—were treated identically. To prepare oligomers, the peptide was solubilized at 1 mg·mL^{-1} in 1,1,1,3,3,3-hexafluoro-2-propanol > 99.0% (Fluka, Sigma-Aldrich Company Ltd., Dorset, UK), and the mixture was vortexed vigorously for 60 s and sonicated in a 50/60 Hz bath sonicator for 5 min. The solvent was removed using dry nitrogen, and the peptidic films were vacuum

(12) Sgourakis, N. G.; Yan, Y.; McCallum, S.; Wang, C.; Garcia, A. E. *J. Mol. Biol.* **2007**, *368*, 1448–1457.

(13) Fishman, P. H.; Brady, R. O. *Science* **1976**, *194*, 906–915.

(14) Hakomori, S. *Curr. Opin. Hematol.* **2003**, *10*, 16–24.

(15) Weng, K. C.; Kanter, J. L.; Robinson, W. H.; Frank, C. W. *Colloid Surface B*. **2006**, *50*, 76–84.

(16) Yokoyama, S.; Takeda, T.; Abe, M. *Colloid Surface B*. **2001**, *20*, 361-368.

(17) Yokoyama, S.; Ohta, Y.; Sakai, H.; Abe, M. *Colloid Surface B*. **2004**, *34*, 65–68.

(18) Choo-Smith, L.-P.; Garzon-Rodriguez, W.; Glabe, C. G.; Surewicz, W. K. *J. Biol. Chem.* **1997**, *272*, 22987–22990.

(19) Terzi, E.; Hölzemann, G.; Seelig, J. *Biochemistry* **1994**, *33*, 7434–7441.

(20) Olofsson, A.; Borowik, T.; Gröbner, G.; Sauer-Eriksson, A. E. *J. Mol. Biol.* **2007**, *374*, 186–194.

(21) Knight, J. D.; Williamson, J. A.; Miranker, A. D. *Protein Sci.* **2008**, *17*, 1850–1856.

(22) Knight, J, D.; Miranker, A. D. *J. Mol. Biol.* **2004**, *341*, 1175–1187.

(23) Williamson, J. A.; Loria, J. P.; Miranker, A. D. *J. Mol. Biol.* **2009**, *393*, 383–396.

(24) Pillot, T.; Goethals, M.; Vanloo, B.; Talussot, C.; Brasseur, R.; Vandekerckhove, J.; Rosseneu, M.; Lins, L. *J. Biol. Chem.* **1996**, *271*, 28757–28765.

(25) van Rooijen, B. D.; Claessens, M. A. E.; Subramaniam, V. *Biochim. Biophys. Acta* **2009**, *1788*, 1271–1278.

desiccated for 30 min. The amyloid was resolubilized at $1 \text{ mg} \cdot \text{mL}^{-1}$ with dimethyl sulfoxide > 99.9% (Sigma-Aldrich Company Ltd., Dorset, UK), and the mixture was vortexed vigorously for 60 s and then sonicated for 5 min. A 200 μL portion of the peptide in DMSO was added to a 2 mL Zeba buffer exchange spin column equilibrated with $10 \text{ mmol} \cdot \text{dm}^{-3}$ HEPES, $100 \text{ mmol} \cdot \text{dm}^{-3}$ NaCl, $1 \text{ mmol} \cdot \text{dm}^{-3}$ EDTA, and $0.05 \text{ mmol} \cdot \text{dm}^{-3}$ NaN$_3$, pH 7.4 (all purchased from Sigma-Aldrich Company Ltd., Dorset, UK), from this point referred to as HEPES pH 7.4. Once absorbed into the column resin, a 40 μL stacker of 0.22 μm filtered water was added to the column. The column was spun in a 4 °C controlled Mikro 22R centrifuge (Hettich UK, Manchester, UK) at 1000 g for 2 min. The eluted peptide was centrifuged in a 4 °C controlled Eppendorf microcentrifuge (Eppendorf UK Ltd., Cambridge, UK) at 16 000 g for 30 min to remove contaminants and preformed fibrillar material. The supernatant was placed in a clean nonstick microcentrifuge tube and kept at 4 °C until use to minimize fibrillization. This is referred to as "zero hour" incubated Aβ. The concentration was determined using a molar extinction coefficient of $1490 \text{ M}^{-1} \cdot \text{cm}^{-1}$ and the absorbance was measured at a wavelength of 280 nm using an Eppendorf Biophotometer (Eppendorf UK Ltd., Cambridge, UK). Stock peptide concentrations of 100–130 μmol $\cdot$ dm^{-3} resulted from the above preparations and were incubated at these concentrations for all experiments. Upon timed incubations, the peptide stocks were diluted to the 10 μmol $\cdot$ dm^{-3} working concentrations directly into the LUVs. It has been noted that the solubilization of amyloid peptides using HFIP can cause neurotoxic ion flux through cellular membranes, as residues of the solvent can cause gradual thinning of the membranes, which results in a concomitant increase in transmembrane current.[26] However, the above preparation ensures all residual HFIP has been evaporated and DMSO has been replaced with buffer. Complete removal of DMSO and HFIP was confirmed by the absence of characteristic solvent signals in the ^{1}H and ^{19}F NMR spectra respectively.

Biomimetic Membrane Constituents. The composition of the LUVs was adapted from a previous study looking at cholera–membrane interactions by surface plasmon field enhanced fluorescence spectroscopy, to contain physiologically relevant proportions of cholesterol and GM1.[27] 1,2-Dimyristoyl-*sn*-glycero-3-phosphocholine (DMPC) was purchased from Avanti Polar Lipid, Inc. (Alabaster, AL, US). Cholesterol, 95%, and monosialoganglioside G$_{M1}$ from bovine brain, > 95% lyophilized powder, was purchased from Sigma-Aldrich Company Ltd. (Dorset, UK). All materials were used without further purification.

Calcein-Encapsulated Unilamellar Lipid Vesicles. The 40 mg $\cdot$ mL^{-1} stock solutions of DMPC, cholesterol, and GM1 were solubilized in 2:1 chloroform/methanol and stored in clean glass vials at −20 °C. Lipid films were prepared by making 68:30:2 DMPC/cholesterol/GM1 aliquots, then the solvent was removed using nitrogen. The films were placed in a vacuum desiccator overnight to ensure complete removal of the solvents. The dry lipid films were rehydrated to 10 mg $\cdot$ mL^{-1} with 200 mmol $\cdot$ dm^{-3} calcein pH 7.4 (Sigma-Aldrich Company Ltd., Dorset, UK), and the mixtures were vortexed vigorously for 30 min. The resulting suspension was passed 19 times through an Avestin extruder fitted with two stacked 100 nm polycarbonate membranes (GC Technology Ltd., Bedford, UK). Nonencapsulated calcein was removed from the LUVs using a slightly modified minicolumn preparation.[28] Briefly, 200 μL of liposome suspension was added dropwise to the top of a 1 mL sephadex G-50 minicolumn, and a 40 μL stacker of 0.22 μm filtered water was applied to the

G-50 column. When the gel matrix had absorbed the liposome suspension, the column was spun in a 4 °C controlled Mikro 22R centrifuge at 2000 rpm for 3 min to dispel the LUVs into the centrifuge tube. The eluted LUVs were washed a further two times using fresh G-50 columns to ensure all nonencapsulated calcein had been removed. The 10 mg $\cdot$ mL^{-1} three-times-washed 100 nm LUVs were diluted to 1 mg $\cdot$ mL^{-1} in HEPES pH 7.4 and were stored at 4 °C until use. GM1-negative LUVs comprised of DMPC/cholesterol at a ratio of 70/30, respectively, and were prepared as above. The encapsulation of calcein was checked in the fluorimeter by checking the release of the self-quenched calcein upon the addition of excess triton X-100. If the calcein intensity did not exceed 100% of the starting fluorescence intensity prior to triton addition, then the LUVs were discarded.

Fluorescence Spectroscopy. Fluorescence measurements were carried out on a Varian Cary Eclipse Fluorimeter (Varian Ltd., Oxford, UK). Samples were placed in a 1 cm path length quartz cuvette (Starna, Essex, UK), and the calcein fluorescence was monitored at various time points using an excitation wavelength of 490 nm. Calcein emission was monitored between 500 and 600 nm, with maximum fluorescence intensity at around 520 nm at a controlled temperature of 20 °C. Excitation and emission slits were both set to 10 nm, and the scan rate was set to 100 nm/min with 0.833 nm data intervals and an averaging time of 0.55 s. The photomultiplier tube detector was set to low to ensure the PMT was not overexposed. Experiments were carried out in duplicate to confirm trends. Fluorescence intensities at the peak of 520 nm were plotted against time.

Transmission Electron Microscopy. A 4 μL droplet of the peptide (100–130 μmol $\cdot$ dm^{-3}) was adsorbed onto Formvar/carbon coated 400 mesh copper grids (Agar Scientific, Essex, UK) for 60 s, and blotted dry. 4 μL of 0.22 μM in water was added to the grid and immediately blotted, then negatively stained with 4 μL of 2% w/v uranyl acetate was adsorbed for 60 s and blotted dry. The grid was allowed to air-dry before examination on a Hitachi 7100 microscope (Hitachi, Germany) fitted with a Gatan Ultrascan 1000 CCD camera (Gatan, Abingdon, UK). Aliquots of samples at the stock concentration were taken at time points for each experiment to monitor fibrillization state and morphology. Measurements were made using ImageJ.[29]

Circular Dichroism. Aβ was resuspended at a concentration of 200 μmol $\cdot$ dm^{-3} in 10 mmol $\cdot$ dm^{-3} HEPES, 100 mmol $\cdot$ dm^{-3} NaF, 1 mmol $\cdot$ dm^{-3} EDTA, and 0.05 mmol $\cdot$ dm^{-3} NaN$_3$, pH 7.4 using the same protocol as previously discussed. CD spectra were collected using a Jasco J715 spectrometer (Jasco Inc., MA, USA) between 320 and 180 nm using a 0.05 cm path length squash cell (Starna Scientific Ltd., UK). Three scans were collected and averaged for each sample at a scan rate of 100 nm/minute, with a 4 s response, 100 millidegree sensitivity, data pitch of 0.1 nm, and a 1 nm bandwidth. The signal for the buffer was subtracted from each scan to account for any inherent buffer circular dichroic signal. Raw data was processed and converted into molar ellipticity (degrees $\cdot$ cm^2 $\cdot$ dmol^{-1}).

Results and Discussion

Characterization of Aβ42 Assembly by Electron Microscopy and Circular Dichroism. Soluble Aβ42 was prepared as described in the methods section and was allowed to assemble in the absence of lipid vesicles, and the aggregates were examined at particular time points by electron microscopy to observe the fibrillization process (Figure 1a). Micrographs show a variety of morphologies, which include small amorphous aggregates, small circular oligomers, and short protofibrils. The size of the initial amorphous Aβ range between 10 and 70 nm in diameter and show heavier negative staining compared to the structured Aβ.

(26) Capone, R.; Quiroz, F. F.; Prangkio, P.; Saluja, I.; Sauer, A. M.; Bautista, M. R.; Turner, R. S.; Yang, J.; Mayer, M. *Neurotox. Res.* **2009**, *16*, 1–13.

(27) Williams, T. L.; Jenkins, A. T. A. *J. Am. Chem. Soc.* **2008**, *130*, 6438–6443.

(28) New, R. R. C. *Liposomes: A Practical Approach*, New, R. R. C, Ed.; IRL Press: Oxford, 1990; pp 130−131.

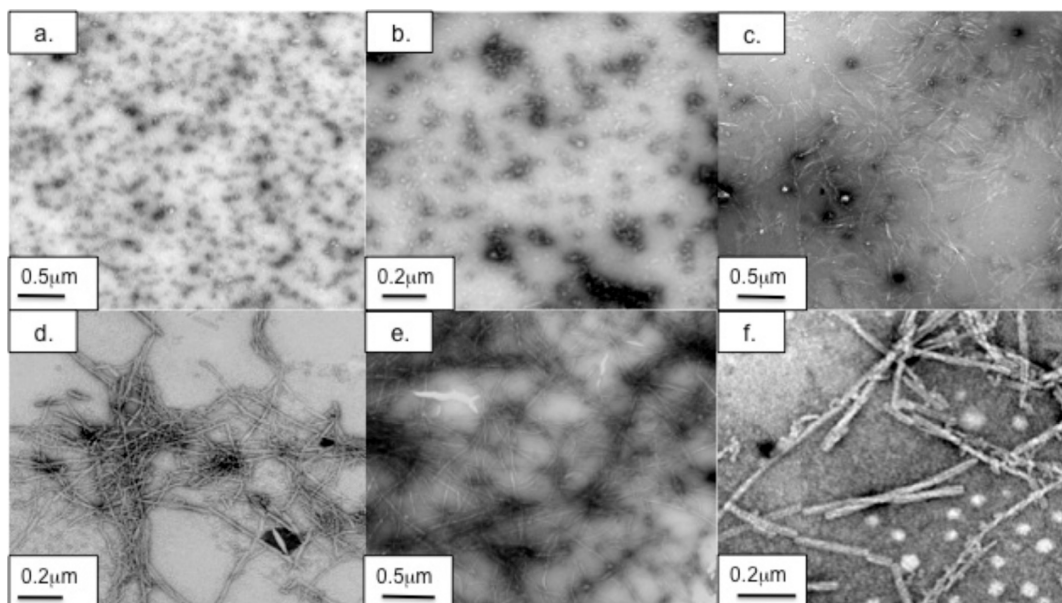(29) Abramoff, M. D.; Magalhaes, P. J.; Ram, S. J. *Biophotonics Intl.* **2004**, *11*, 36–43.

Figure 1. Transmission electron micrographs showing negatively stained Aβ42 assembly. Time course shows the results of 100 μmol·dm^{-3} Aβ42 assembled in vitro after incubation for time periods of (a) 0 h, (b) 1 h, (c) 3 h, (d) 48 h, (e) 72 h, and (f) 168 h.

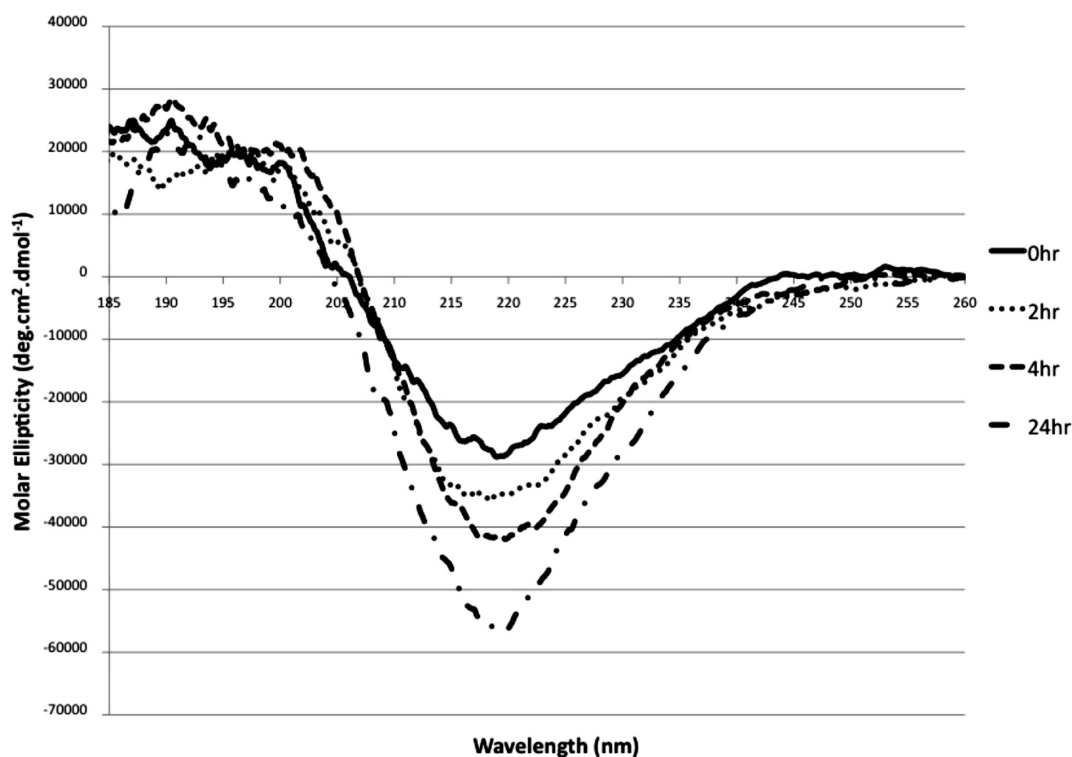**Figure 2.** Circular dichroism spectra of assembling Aβ42. The time course shows the results of in vitro assembly of 200 μmol·dm^{-3} Aβ42 at 20 °C, in a 0.05 cm path length squash-cell cuvette at time: 0 h (—), 2 h (· · ·), 4 h (− − −), and 24 h (− · − · −).

The amorphous peptide aggregates into larger 100−200 nm structures within 60 min (Figure 1b), whereby the smaller amorphous Aβ clustered to form masses. The secondary structure of the zero hour incubated Aβ42 was monitored by circular dichroism and shows a characteristic signal at 218 nm, indicative of a β-sheet structure (Figure 2). This increases in intensity as fibrils formed at 24 h, suggesting that the proportion of β-sheet within the solution increases with time. By electron microscopy, the amorphous aggregates increase in numbers up until 2 h, at which time, short protofibrils between 15 and 80 nm in length and

high molecular weight oligomers with a diameter between 1 and 5 nm emerge (Figure 1c). Circular dichroism spectra indicate that the Aβ solution increases in β-sheet content as the sample becomes more ordered and fibrillar (Figure 2). Oligomeric Aβ became the minor species as distinct fibrillar structures appear after 3 h of incubation. As the fibers mature, their morphology changes, and they become elongated with more defined edges. Fibril length becomes indeterminate after 4 h, whereas fibril width increases to between 6 and 18 nm at 48 h (Figure 1d), to 14−18 nm at 72 h, and then to 16−22 nm at 168 h. Polymorphism is observed during the
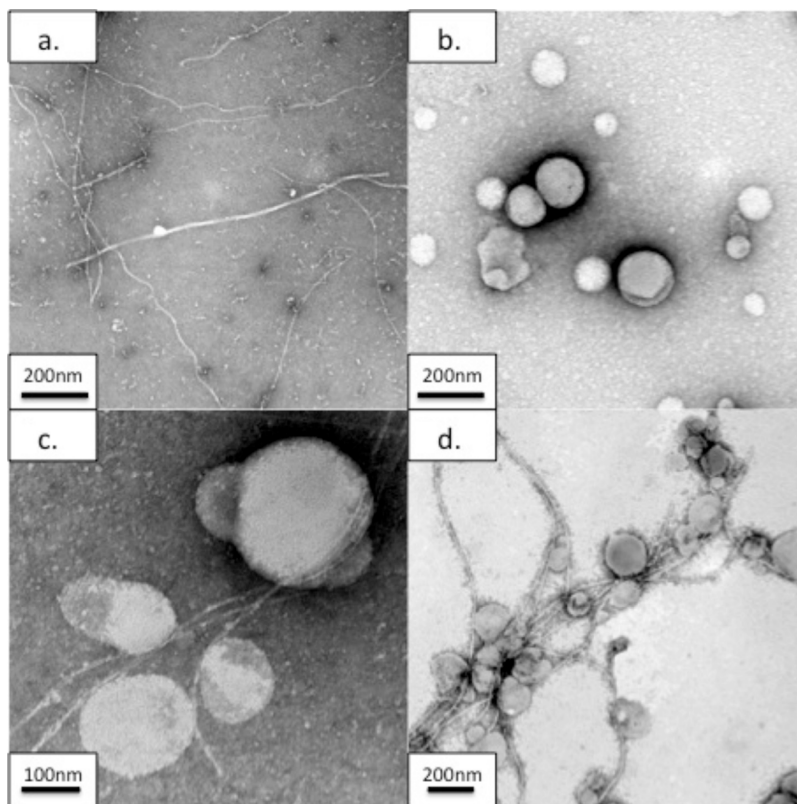
Figure 3. Transmission electron micrographs showing negatively stained Aβ42 fibers at 72 h incubation, LUVs, and Aβ42-associated LUVs. Showing Aβ42 fibrillization in the presence of biomimetic membranes. (a) $100 \, \mu mol \cdot dm^{-3}$ Aβ42 alone after 72 h. (b) $1 \, mg \cdot mL^{-1}$ LUVs alone. $10 \, \mu mol \cdot dm^{-3}$ zero hour Aβ42 and $1 \, mg \cdot mL^{-1}$ LUVs incubated together for 72 h (c and d).

maturation of fibers and within the fiber population. Striated, ribbon-like fibers that show irregular twisting are seen earlier in the fibrillization (4 h) compared to left-handed regularly twisted fibers that are only observed after 24 h and appear as the minor morphology (Figure 1d−f). The structural polymorphism of Aβ42 fibrils has also been shown in other amyloid forming peptides such as amylin,[30] glucagon,[31] and Aβ40.[32] Polymorphism has been implicated to arise from various exogenous factors such as buffer composition, temperature, and peptide concentration. Agitation of the peptide solution during fibrillization predominantly produced fibril filaments with no resolvable twists that laterally associated into multimers, whereas quiescently produced Aβ40 fibrils demonstrated periodic modulations in their fibril widths.[33]

To ensure that the presence of lipids did not adversely affect the fibrillization of Aβ and to visually confirm that Aβ produces similar fibers in the presence and absence of lipids, transmission electron micrographs were prepared of LUVs incubated with zero hour Aβ42 for 72 h. Fibrillization of Aβ42 proceeds in the presence of lipids, and produces long, unbranched fibers with the same fibrillar width as fibers produced in the absence of lipids (Figure 3). However, the fibers appear to cause changes in the vesicle morphology from typically spherical vesicles with apparently smooth lipid bilayers between 90 and 160 nm (Figure 3b), to

more irregularly shaped, rough vesicles between 119 and 210 nm that have blebs protruding around the membranes (Figures 3c and d). Therefore, it would appear that the presence of Aβ causes changes in membrane structure, possibly by bringing the vesicles into close proximity with each other and thereby allowing them to fuse more readily, the growing of the fiber on or within the membrane may cause perturbation of the lipid bilayer, or the formation of defects within the membrane allowing the swelling of the LUVs.

Aβ42-Induced Permeation of Membranes. To examine the effect of assembling Aβ42 on synthetic lipid vesicles, soluble Aβ42 was prepared in HEPES pH 7.4 at a concentration of ∼100−130 $\mu mol \cdot dm^{-3}$ (known from here on as zero hour incubated Aβ) and then added to $1 \, mg \cdot mL^{-1}$ calcein-encapsulated lipid vesicles to a final peptide concentration of $10 \, \mu mol \cdot dm^{-3}$. The calcein fluorescence was monitored at 520 nm to observe the permeation of the membrane as a result of the addition of Aβ. The change in calcein fluorescence was monitored every 15 min for 60 min (Figure 4a) and then every 24 h over a 96 h period to observe the prolonged incubation of the peptide with the lipid membranes (Figure 4b). Concurrently, transmission electron micrograph grids were prepared to visualize the fibrillization state of Aβ at the stock preparation concentration (100−130 $\mu mol \cdot dm^{-3}$) (Figure 1). The addition of Aβ42 to LUVs caused an immediate 6-fold increase in the rate of calcein efflux compared to natural membrane diffusion (Figure 4a). Aβ42 induced permeation increased to a 10-fold rate within 15 min of monitoring the fluorescence signal. Following the initial burst between 0 and 60 min, the rate of Aβ-induced permeation decreased from 24 h, when the rate of permeation became constant (Figure 4b). The permeation of the lipid vesicles appears to follow a two-stage process, whereby the majority of calcein leakage is observed

(30) Goldsbury, C. S.; Cooper, G. J.; Goldie, K. N.; Müller, S. A.; Saafi, E. L.; Gruijters, W. T.; Misur, M. P.; Engel, A.; Aebi, U.; Kistler, J. *Struct. Biol.* **1997**, *119*, 17–27.

(31) Pedersen, J. S.; Dikov, D.; Flink, J. L.; Hjuler, H. A.; Christiansen, G.; Otzen, D. E. *J. Mol. Biol.* **2006**, *355*, 501–523.

(32) Meinhardt, J.; Sachse, C.; Hortschansky, P.; Grigorieff, N.; Fändrich, M. *J. Mol. Biol.* **2009**, *386*, 869–877.

(33) Petkova, A. T.; Leapman, R. D.; Guo, Z.; Yau, W.-M.; Mattson, M. P.; Tycko, R. *Science* **2005**, *307*, 262–265.
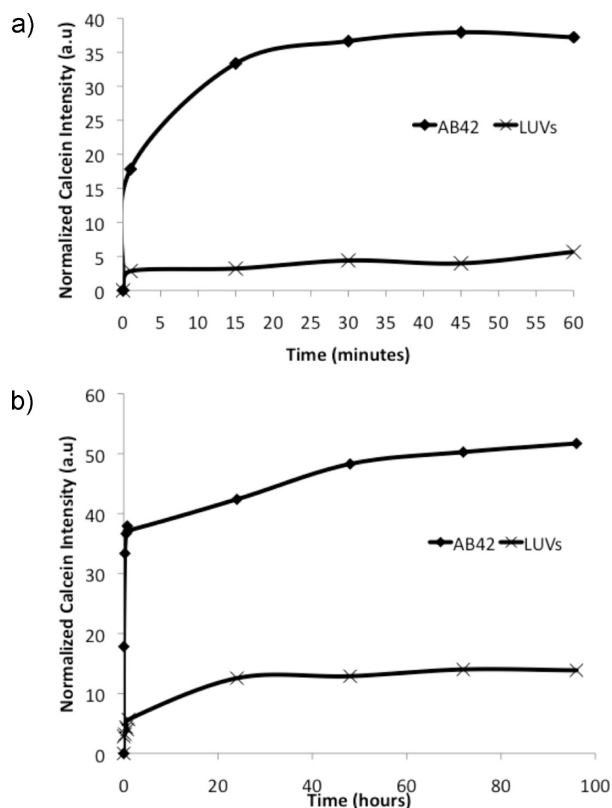
Figure 4. Calcein fluorescence emission showing the effect of Aβ42 on LUVs with time. (a) fluorescence spectra were measured at 520 nm and show results from LUVs (1 mg·mL^{-1}) encapsulating[3] calcein (200 mmol·dm^{-3}) upon addition of 10 μmol·dm^{-3} Aβ42 at time = 0 h (♦), compared to the natural leakage of LUVs (×) from 0 to 60 min; (b) measurement of fluorescence from untreated LUVs (×), which does not change after > 24 h, while Aβ42 continues to permeate the membranes until the end of the measurement at 96 h (♦).

during the initial 60 min (Figure 4a) of peptide-vesicle incubation (65% of the total calcein diffusion occurred within initial 60 min). This is followed by slower calcein efflux until leakage begins to plateau after 48 h (Figure 4b). This seems to indicate that the early assemblies interact with the membrane and effectively increase in concentration on the membrane surface as they begin to aggregate and fibrillize, and this results in leakage of dye from the vesicles. Alternatively, the two-stage permeation maybe due to heterogeneity of the amyloid sample, whereby the initial fast efflux results from a highly toxic species and the second phase is the result of less toxic species. As a control, natural membrane diffusion without addition of peptide was also monitored over several days (Figure 4a and b).

Comparison of Wild-Type and Mutant Aβ Permeation of Membranes. *Aβ42-Initiated Membrane Permeation*. In this section of the study, Aβ variants were incubated in HEPES pH 7.4 for 0, 1, 2, 3, 4, 24, 48, 72, and 96 h, and *then* added to a final concentration of 10 μmol·dm^{-3} to freshly prepared LUVs. The calcein fluorescence signal was monitored to observe the peptide-induced leakage as a consequence of addition of the peptide samples. Figure 5 shows the effect of Aβ variant incubation time on membrane leakage. Transmission electron micrographs were prepared concurrently to show the assembly state of Aβ variants at the incubation time points.

The addition of zero hour incubated Aβ42 caused the greatest amount of calcein leakage and showed an immediate increase in calcein fluorescence within the initial 60 min of observation
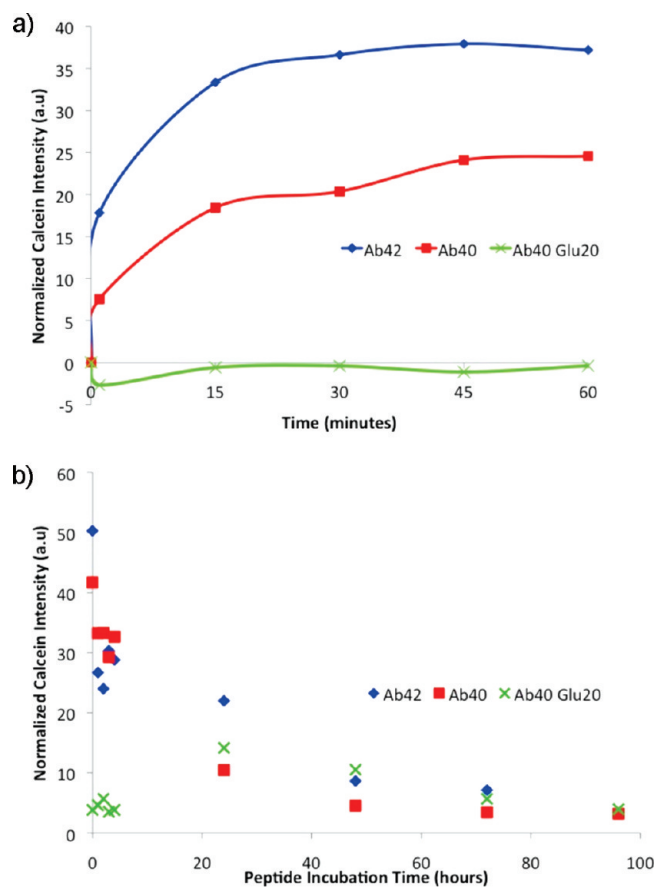

Figure 5. Calcein fluorescence emission showing the initial effect (0−60 min) of Aβ42, Aβ40, and Aβ40 Glu20 incubation time on LUVs (a) and prolonged incubation over 96 h (b). Calcein fluorescence emission time course at 520 nm showing the effect of preincubated peptides on LUVs encapsulating calcein. (a) The initial LUV permeation from 0 to 60 min by Aβ42 at time = 0 h (♦), Aβ40 at time = 0 h (■), and Aβ40 Glu20 at time = 0 h (×). (b) Aβ42 (♦), Aβ40 (■), and Aβ40 Glu20 (×) were quiescently incubated at room temperature for 0, 1, 2, 3, 4, 24, 48, 72, and 96 h in HEPES pH 7.4 before addition to the LUVs at a final peptide concentration of 10 μmol·dm^{-3} and monitoring of the calcein fluorescence until 96 h.

(Figure 5a). At this time, Aβ42 was observed by TEM to form oligomeric species composed of some circular oligomers, high molecular weight oligomers, and short protofibrils (Figure 6a). As the peptide begins to aggregate, the ability of the peptide to cause membrane permeation declines. The addition of Aβ42 incubated for times between 1 and 24 h caused 50% less calcein leakage compared to Aβ42 incubated for 0 h (Figure 5b and 7). Incubation of the peptide for times greater than 48 h, when fibrils are clearly observed by TEM (Figure 1), showed 80% less membrane leakage compared to zero hour incubated Aβ42 (Figure 5b). No observable membrane permeation was observed upon addition of 96 h incubated Aβ42 (Figure 7), at which time transmission electron micrographs showed the peptide had fibrillized into long, unbranched mature fibrils (Figure 6c and Figure 1f). This demonstrates that it is the early oligomeric species that cause the most membrane permeation (Figure 7), and this has not previously been shown for Aβ42. It is important to consider that this could be due to the larger number of molecules of oligomers available in solution when compared to fibril molecules, with shorter assemblies providing more ends. This is supported by the recent findings of the Radford group, which found that fragmentation of
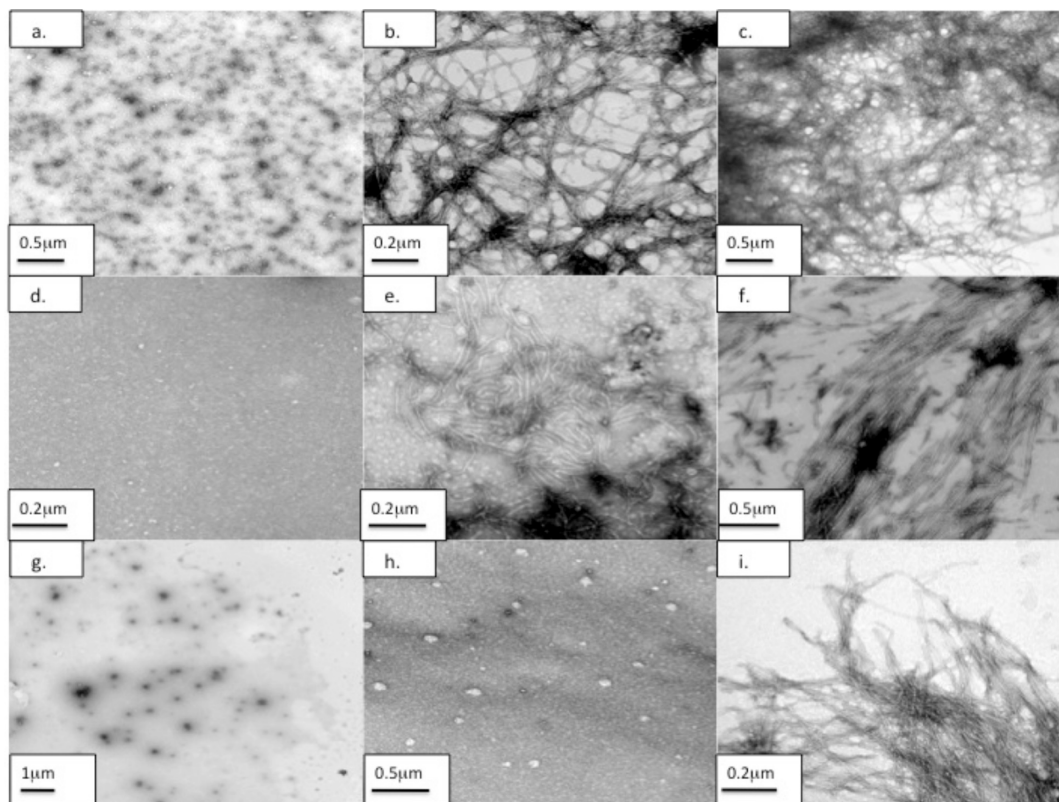
Figure 6. Transmission electron micrographs showing negatively stained Aβ42, Aβ40, and Aβ40 Glu20 assembly. Transmission electron micrographs of Aβ42 following incubation for (a) 0 h, (b) 24 h, and (c) end point. Aβ40 incubation for (d) 0 h, (e) 24 h, and (f) end point. Aβ40 Glu20 incubation for (g) 0 h, (h) 24 h, and (i) end point.
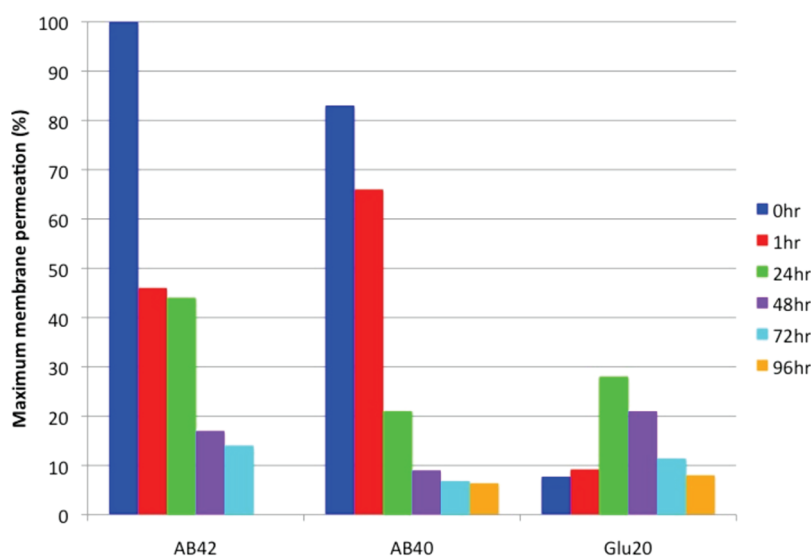

Figure 7. Percentage calcein fluorescence emission showing the effect of Aβ variant incubation time on LUVs as a function of Aβ42 maximal permeation. Comparison of the membrane permeation effects of Aβ variants as a function of peptide incubation time. Percentage membrane permeation is plotted relative to the maximum leakage measured for Aβ42 (at time = 0 h), which is normalized to 100%. Membrane permeation is measured by the fluorescence arising from calcein release.

β$_2$-microglobulin fibers into shorter fibril fragments caused significant membrane permeation of lipid vesicles and cell cytotoxicity compared to fully matured fibers.[34] It was suggested that fragmentation of the β$_2$-microglobulin fibers caused fewer fibril−fibril interactions, thereby allowing more

fibril−membrane interactions to occur. The conformational dependence of Aβ42 induced neurotoxicity has previously been reported in human cortical neurons, and it was demonstrated that low concentrations (5 μmol·dm^{-3}) of oligomeric Aβ42 caused greater toxicity compared to fibrillar Aβ42.[35] Busciglio

(34) Xue, W.-F.; Hellewell, A. L.; Gosal, W. S.; Homans, S. W.; Hewitt, E. W.; Radford, S. R. *J. Biol. Chem.* **2009**, *284*, 34272–34383.

(35) Deshpande, A.; Mina, E.; Glabe, C.; Busciglio, J. *J. Neurosci.* **2006**, *26*, 6011–6018.

showed that fibrillar Aβ caused progressive abnormal cell development and reduced cell death compared to oligomeric Aβ42 and Aβ-derived diffusible ligands. Oligomeric α-synuclein (0.13 μmol·dm^{-3}) was shown to cause more calcein leakage of negatively charged phosphatidylglycerol vesicles compared to monomeric and fibrillar α-synuclein, which only caused membrane permeation at much higher concentrations of 21 and 7 μmol·dm^{-3}, respectively.[25]

Aβ40-Initiated Membrane Permeation. The addition of zero hour incubated Aβ40 to vesicles caused immediate calcein leakage (Figure 5). Zero hour Aβ40 caused 33% less calcein leakage compared to Aβ42 within the initial 60 min of incubation (Figure 5 inset) and 20% less membrane damage compared to Aβ42 over the course of the whole experiment (Figure 7). Calcein leakage was significantly reduced as Aβ40 became fibrillar, and peptide incubated for times over 48 h showed little ability to cause permeation (Figure 7). This demonstrates that Aβ42 causes more membrane permeation compared to Aβ40 when incubated for the same length of time, despite the slower assembly kinetics of Aβ40.

As Aβ40 assembled to form higher molecular weight aggregates, its ability to cause membrane permeation decreased. Aβ40 incubated for 1, 24, and 96 h caused 20, 60, and 70% less calcein leakage, respectively, compared to zero hour incubated Aβ40 (Figure 7). TEM images revealed that zero hour incubated Aβ40 were observable as circular entities with diameters between 6 and 14 nm. Higher molecular weight oligomers with diameters between 10 and 40 nm were observed with Aβ40 incubated for 4 h (Figure 6e). Protofibrillar, curvilinear, and short fibrils of Aβ40 were not observed until 24 h of peptide incubation, whereas long, fully formed fibers were only observed from 72 h (Figure 6f).

Aβ40 Glu20-Initiated Membrane Permeation. The addition of zero hour incubated Aβ40 Glu20 to the biomimetic membranes caused little membrane permeation. Incubation of the Aβ40 Glu20 variant for times less than 24 h resulted in no significant change in calcein intensity. The negative values observed in the inset of figure 5 are not significant, and is the outcome of normalizing the results against the initial LUV calcein fluorescence, as there is always a small deviation between LUV aliquots from the same sample due to slight variations in vesicle encapsulation efficiencies. Interestingly for this slower assembling variant, membrane permeation was observed after the addition of Aβ40 Glu20 that had been incubated for 24 h. However, the maximal membrane leakage for Aβ40 Glu20 was 70% lower than that observed with Aβ42 at the same incubation time, and peptide incubated for 48 h resulted in 80% less membrane permeation compared Aβ42 (Figure 7). The ability to cause maximal membrane permeation at a peptide incubation time of 24 h was reproducible. Transmission electron micrographs of zero hour incubated Aβ40 Glu20 showed a range of morphological species ranging from small circular entities between 5 and 15 nm in diameter to short protofibrillar rods that were around 5 nm in diameter and were 10−40 nm in length (Figure 6g). At 24 h, Aβ40 Glu20 structures were similar to earlier time points by electron microscopy (Figure 6h). A small number of short, striated fibers (40 nm in width, 200 nm in length) emerged after 48 h of peptide incubation; however, they were a very small proportion of the observed peptide population. Fibrillar peptide became apparent after 120 h incubation, and TEM images showed the fibers had a width of less than 10 nm and their lengths could not be determined (Figure 6i). As predicted by aggregation propensity studies, Aβ42 Glu20 does slowly aggregate and was observed to fibrillize four times slower than wild-type Aβ42.[19] The ability of Aβ40 Glu20 to cause calcein leakage after 24 h incubation suggests an intermediate aggregate that precedes the appearance of TEM
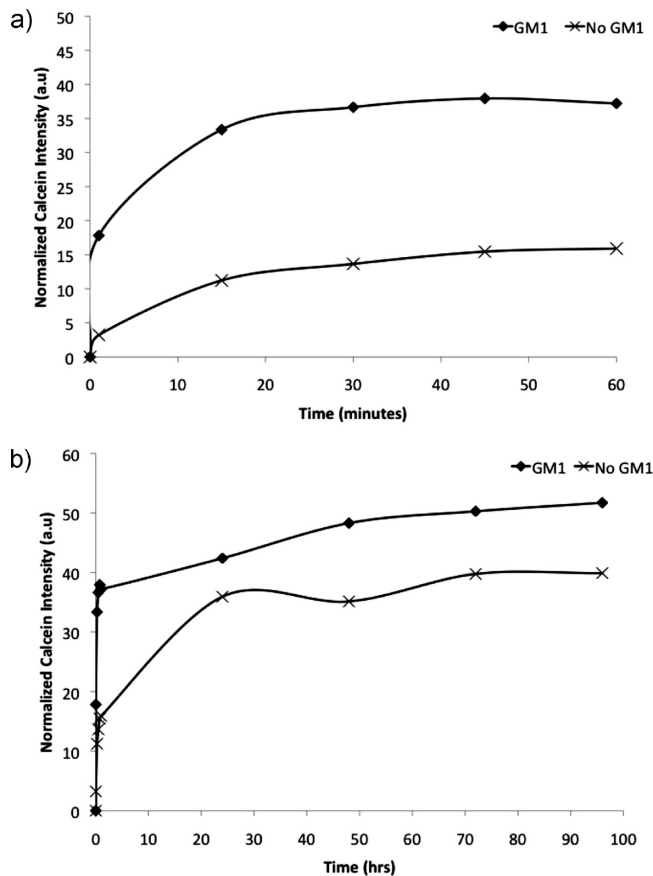

Figure 8. Calcein fluorescence emission showing the effect of GM1 ganglioside on Aβ42 permeation of LUVs. (a) shows the initial LUV permeation from 0 to 60 min by Aβ42 at time = 0 h of DMPC/cholesterol LUVs (♦) compared to the permeation to DMPC/cholesterol/GM1 LUVs (×) between 0 and 60 min. (b) Aβ42 was quiescently incubated at room temperature for 0, 1, 2, 3, 4, 24, 48, 72, and 96 h in HEPES pH 7.4 before addition to the LUVs at a final peptide concentration of 10 μmol·dm^{-3} and monitoring of the permeation of 1 mg·mL^{-1} DMPC/cholesterol LUVs (♦) compared to the permeation to DMPC/cholesterol/GM1 LUVs (×) between 0 and 96 h.

observable fibrillar peptide was responsible for membrane permeation. This result also supports the view that a specific assembly of Aβ molecules results in membrane binding and permeation, rather than monomeric Aβ. Indeed, we do not believe the 0 h Aβ42 or Aβ40 preparations are necessarily monomeric by the time they are added to the membrane models, and this is supported by the β-sheet signal evident from CD experiments.

Significance of GM1 Ganglioside on Aβ Permeation of Membranes. We were interested in investigating the importance of GM1 within the lipid bilayer toward Aβ42 membrane permeation. The addition of 10 μmol·dm^{-3} Aβ42 to LUVs excluding GM1 (70:30 DMPC/cholesterol) caused leakage of the encapsulated calcein (Figure 8). However, membrane permeation was significantly reduced compared to the addition of 10 μmol·dm^{-3} zero hour incubated Aβ42 to LUVs containing GM1 (68:30:2 DMPC/cholesterol/GM1). A 57% reduction in calcein leakage from GM1-excluded LUVs was observed over the initial 60 min of peptide-membrane incubation (Figure 8a). Over an extended time period, the overall reduction in calcein leakage was 20% less compared to GM1-containing LUVs (Figure 8b). This suggests that GM1 has an effect on Aβ-induced membrane permeation

and could indicate that GM1 has a relevant physiological effect in amyloid-induced toxicity.

The interaction between GM1 and Aβ at pH 7.4 would not principally result from electrostatic interactions since Aβ42 has a calculated net charge of −2.9 (Protein Calculator v3.3, The Scripps Research Institute), and GM1 has a negative charged sialic acid moiety on the headgroup.[36] Therefore, the interaction between Aβ and GM1 would be expected to repel one another at pH 7.4. However, the addition of sodium chloride has been shown to shield these repulsive electrostatic forces, effectively allowing the insertion of Aβ into the lipid bilayer.[37] Hydrophobic interactions play a greater role in Aβ-membrane binding, whereby a solvent-exposed aromatic residue stacks onto a sugar ring of the glycolipid (CH-π stacking interaction). The stacking interaction is driven by net positive charge of the sugar ring in proximity to the π-electron cloud of the amino acid aromatic ring.[38] The polar moiety of the glycolipid GM1 receptor provides a complementary surface for polar amino acids for the formation of hydrogen bonds. Moreover, the decrease in glucosylceramide synthase activity in aged and Alzheimer's diseased brains, which regulates ceramide levels and therefore ganglioside levels,[39] suggests a link to the increase in proportion of gangliosides with age. Ganglioside levels were shown to increase with age in brain regions of transgenic mouse models.[40] Therefore, an increase in ganglioside content in plasma membranes may increase the propensity of Aβ permeation of neuronal membranes as the gangliosides confer an increase in the electronegativity to the membranes.

Conclusions

It is well know that Aβ42 assembles to form increasingly large assemblies that eventually form mature amyloid fibrils. The early, assembled species have been implicated in cytotoxicity and it has been suggested that the small size allows the assemblies to interact with, or pass through the cell membrane. Here we have shown that Aβ42 has the ability to cause permeation of synthetic membranes and that this ability decreases as assembly progresses. We show that the appearance of small, spherical aggregates correlates best with the membrane disruption activity. Comparison with the less fibrillogenic and less toxic Aβ40 and with the poorly fibrillogenic Aβ40 Glu20 variant reveals that these have a lesser ability to cause permeation and that this ability also appears to be dependent on the assembly state of the peptide. In this work, we definitively show that small oligomeric species cause membrane permeation, whereas fibrillar aggregates have a significantly reduced ability to induce membrane leakage. Finally, GM1 may play a role in the binding of Aβ to the membrane, since removal significantly decreases permeation by Aβ42. Overall, this work supports the view that small assemblies of Aβ can interact with membranes and disrupt membrane integrity, and this may be an important step in cytotoxicity and therefore in disease progression.

Glossary

Aβ	amyloid-β peptide
Aβ40	amyloid-β peptide1−40
Aβ42	amyloid-β peptide1−42
Aβ40 Glu20	amyloid-β peptide1−40 phenylalanine/20/glutamic acid variant
AD	Alzheimer's disease
APP	amyloid precursor protein
CD	circular dichroism
DMPC	1,2-dimyristoyl-*sn*-glycero-3-phosphocholine
DMSO	dimethyl sulfoxide
EDTA	ethylenediaminetetraacetic acid
GM1	monosialoganglioside G_{M1}
GUV	giant unilamellar vesicles
HEPES	4-(2-Hydroxyethyl)piperazine-1-ethanesulfonic acid, N-(2-Hydroxyethyl)piperazine-N′-(2-ethane-sulfonic acid)
HFIP	1,1,1,3,3,3-hexafluoro-2-propanol
IAPP	islet amyloid polypeptide
K_D	equilibrium dissociation constant
LUV	large unilamellar vesicles
Met35	methionine residue 35
NaCl	sodium chloride
NaN_3	sodium azide
NMR	nuclear magnetic resonance
RPM	revolutions per minute

(36) McDaniel, R. V.; McLaughlin, A.; Winiski, A. P.; Eisenberg, M.; McLaughlin, S. *Biochemistry* **1984**, *23*, 4628–4624.

(37) Chi, E. Y.; Frey, S. L.; Lee, K. Y. C. *Biochemistry*. **2007**, *46*, 1913–1924.

(38) Levy, M.; Garmy, N.; Gazit, E.; Fantini, J. *FEBS. J.* **2006**, *273*, 5724–5735.

(39) Marks, N.; Berg, M. J.; Saito, M.; Saito, M. *Brain. Res.* **2008**, *1191*, 136–147.

(40) Barrier, L.; Ingrand, S.; Damjanac, M.; Bilan, A. R.; Hugon, J.; Page, G. *Neurobiol. Aging* **2007**, *8*, 1863–1872.